Advanced Ceramics Progress: Vol. 10, No. 2, (Spring 2024) 1-8

Materials and Energy Research Center
MERC

Contents lists available at ACERP

Advanced Ceramics Progress

Journal Homepage: www.acerp.ir

Original Research Article

Effect of Processing Parameters and Additives on Partially Sintering of Si_3N_4-$MoSi_2$ Composite

Seyed Ali Tayebifard

Associate Professor, Department of Semiconductors, Materials and Energy Research Center, Karaj, Iran.

*Corresponding Author Email: a.tayebifard@merc.ac.ir (S. A. Tayebifard)

URL: https://www.acerp.ir/article_209610.html

ARTICLE INFO

Article History:
Received: 28 April 2024
Revised: 09 September 2024
Accepted: 16 November 2024

Keywords:
Porous Composite,
Si_3N_4,
$MoSi_2$,
Additive,
Paritially Sintered

ABSTRACT

Addition of $MoSi_2$ to Si_3N_4 matrix leads to an improvement in the mechanical properties and oxidation resistance as well as an increase in the electrical conductivity of the produced composite, thus allowing for machining via Electrical Discharge Machining (EDM) or its potential applications as pieces of tinder (igniter) in diesel engines or aerospace devises. In this study, Si_3N_4 powder was mixed with $MoSi_2$ (synthesized in the previous work through SHS) and additives such as MgO, CeO_2, and Y_2O_3 in varying percentages. Some of the mixed powders were milled using a SPEX 8000. All material powders were then formed into pellets using a uniaxial press. The pellets were then sintered in an atmosphere-controlled tube furnace in argon at a maximum temperature of 1500 °C with a soaking time of 2 or 3 hours through Pressureless Sintering (PLS) process. The sintered samples were analyzed at different stages: density measurements, phase and microstructure studies using XRD and SEM, and HV microhardness measurements. The results demonstrated that Si_3N_4-$MoSi_2$ structural porous composites were successfully prepared and optimized by controlled parameters such as pressing pressure, milling process, type and percentage of additives, and soaking times.

https://doi.org/10.30501/acp.2024.453495.1151

1. INTRODUCTION

Two categories of different materials are candidates for stability at working temperatures of approximately 1200 ° C. The first category includes structural ceramics such as SiC and Si_3N_4 while the second one consists of structural silicons such as $MoSi_2$ (Tapia-Lopez et al., 2023). The structural materials based on Si_3N_4 are among the most commonly used ceramics in engineering owing to their unique properties namely thermal shock resistance, thermal resistant under load at high temperature, chemical impartiality, and excellent wear resistance (Singh et al., 2004; Lai et al., 2018; Charfi et al. 2002; Sciti et al., 2002) However, they also exhibit some limitations, including difficult sinterability due to their high-temperature sintering requirement (about 2000°C), decomposition at temperatures above 1900°C, need for improved oxidation resistance under working conditions over a long time (10,000 hours), difficult and costly machining due to their hardness and high electrical resistivity (~ 1014Ωcm), unreliable stability of properties in long-term applications, and insufficient fracture toughness for applications such as engine components. These limitations hinder the industrial use of silicon nitride.

As a result, the Si_3N_4 composites have been developed to improve these properties (Singh et al., 2004). $MoSi_2$ is one of the candidates for constructing composites with Si_3N_4 (Jankowiak et al., 2013; Lizuka et al., 2002). The properties of Silicon Nitride and Molybdenum Disiliide suggest that these two compounds can complement each other. For example, Si_3N_4 has good creep resistance at high temperatures while $MoSi_2$ contributes to toughening at low temperatures and plays a role in the flexural phase at high temperatures in the composite. Additionally, $MoSi_2$ is a conductive material and consequently, after its addition to Si_3N_4, the resulting

Please cite this article as: Tayebifard, S. A.. (2024). Effect of Processing Parameters and Additives on Partially Sintering of Si_3N_4-$MoSi_2$ Composite, *Advanced Ceramics Progress*, 10(2), 1-8. https://doi.org/10.30501/acp.2024.453495.1151

composite can become conductive and machined through Electrical Discharge Machining (EDM) (Singh et al., 2004).

Several synthesis methods have been proposed for preparing this composite, including metallurgical powder, combustion synthesis, two-step method HP/HIP, reaction bonding, combustion synthesis, and infiltration (Liu et al., 2022). Porous ceramics, widely used in different industrial fields such as filters, bioreactors, catalyst carriers, etc. (Yang et al., 2001), have been extensively studied experimentally and theoretically, regardless of their low strain at failure (Kota et al., 2023). Materials based on porous Si_3N_4 with rod-type β-Si_3N_4 grains possess excellent mechanical properties and chemical neutrality (Yang et al., 2001).

In this work, Si_3N_4 and $MoSi_2$ (synthesized through Self-propagating High-temperature Synthesis (SHS) in previous works (Fasihi Dastjerdi, et al., 2012; Shahbazi et al., 2016)) were selected as the raw materials. The structural composites were then produced using powder metallurgy and Pressureless Sintering (PLS). During the study, several parameters such as reactant activation through milling, green compact pressing pressure, and type and percentages of the sintering aids were optimized.

2. MATERIALS AND METHODS

2.1. MATERIALS

Si_3N_4 powder (particle size (45μm)), composed mainly of α-Si_3N_4, purity> 99%, was sourced from Aldrich Company, USA. $MoSi_2$ powder (particle size of 9μm) was synthesized in previous works (Yang et al., 2001; Kota et al., 2023) by SHS. MgO, Y_2O_3 and CeO_2 powders (particle sizes of 3μm), (4μm) and (10μm), respectively) with commercial grade purity, were used as sintering aids.

2.2. COMPOSITE SYNTHESIS

In this step, both Si_3N_4 and $MoSi_2$ synthesized powders (Yang et al., 2001; Kota et al., 2023) were weighted as the main constituents based on a 50/50 vol% ratio. MgO, Y_2O_3 and CeO_2 powders were added individually or together as sintering aids based on Table 1.

Initially, these powders were mixed, and a portion was milled using a Spex 8000 high-energy ball mill. Then all mixed and milled powders were granulated. To prepare the granulate powders, 3wt% Carboxymethyl Cellulose (CMC) binder and a few drops of water were thoroughly mixed, and the mixture was passed through a 40-mesh sieve. In the next step, the granulated powder was pressed into pellets using a uniaxial press at the pressure range of 300-900 MPa. The density of the green compacts was then measured geometrically. Followed by calculating the theoretical density of each sample based on the chemical composition density of its components and mixture of rules in composites, the green relative density of this samples was obtained accordingly. Afterward, the green compact composite samples were sintered in an atmospheric control furnace for the soak time of 2-3 hours at 1500ºC (Ramachandra et al., 2022).

First, the density and porosity of the products were measured using the Archimedes immersion method according to the ASTM C373-88 standard. Finally, the products were analyzed by XRD (Philips, PW3710), SEM (Stereo Scan 360-Leica Cambridge), and microhardness (Akoshi, MVK-H21).

TABLE 1. Introduction of the process parameters, additive, and sample number

Sample No.	Press Pressure (MPa)	Milling Time (h)	Sintering Aid (type & percentage)	Maximum Temperature of Sintering (ºC)	Soaking Time (h)
1	300	0	5wt% MgO	1500	2
2	450	0	5wt% MgO	1500	2
3	600	0	5wt% MgO	1500	2
4	750	0	5wt% MgO	1500	2
5	900	0	5wt% MgO	1500	2
6	600	0	10wt% MgO	1500	2
7	600	1	5wt% MgO	1500	2
8	600	1	10wt% MgO	1500	2
9	600	0	5wt% MgO	1500	3
10	600	1	5wt% MgO	1500	3
11	600	0	10wt% MgO	1500	3
12	600	1	10wt% MgO	1500	3
13	600	0	5wt% MgO + 5wt% CeO_2	1500	3
14	600	1	5wt% MgO + 5wt% CeO_2	1500	3
15	600	0	5wt% Y_2O_3	1500	3
16	600	1	5wt% Y_2O_3	1500	3
17	600	0	10wt% Y_2O_3	1500	3
18	600	1	10wt% Y_2O_3	1500	3

3. RESULTS AND DISCUSSION

3.1. PRESS PRESSURE

The pellets were pressed from the granulate powders using uniaxial press, as mentioned earlier. Figure 1 shows the effect of press pressure on the Relative Density (RD) of the green compacts and final products. As seen in this figure, when the pressure on the granulate powders increases up to 600MPa, the relative density of the green compacts and final products increase. However, if the compression pressure exceeds 900 MPa, the final product densities will not change significantly but the green compact density will decrease.

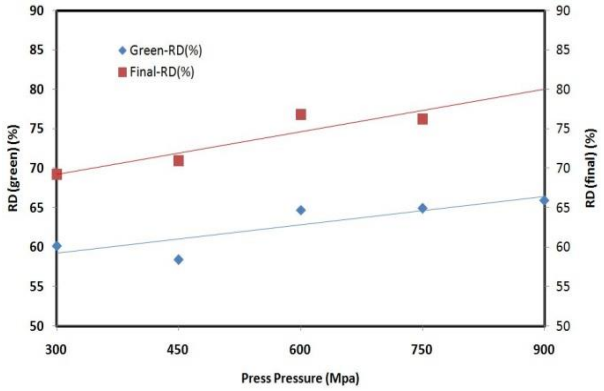

Figure 1. The effect of press pressure on green compacts & final products relative densities (RD). (sintering aid: 5wt% MgO, Max. Temperature: 1500ºC and 2h soaking time)

As noted in the references, increasing press pressure on the powder increases the density of the green compact up to a certain level. Beyond that point, with continues applied pressure, the increase in the green compact density will stop mainly because with higher pressure, there is no more space left in the grain powder to move and slide, thus preventing further density increase. Therefore, increasing pressure beyond a certain level is ineffective in enhancing density (Angelo et al., 2008; German, 2005). After optimizing the compression pressure, the samples were prepared based on the optimal pressure (600MPa) and are referred to in Figure 1.

Figure 2 shows the XRD pattern of the sintered sample. According to this figure, both Si_3N_4 and $MoSi_2$ are the main phases, indicating that the Si_3N_4-$MoSi_2$ composite has been successfully produced.

Figure 3 shows the microstructure of the fracture surface of this sample at two magnifications. This figure reveals a relatively homogenized microstructure with high porosity. However, upon closer examination, a dual morphology of coarse and fine grains can be detected. The grain boundaries of the coarse grain exhibit a curved shape, confirming the formation of liquid phase during the sintering process.

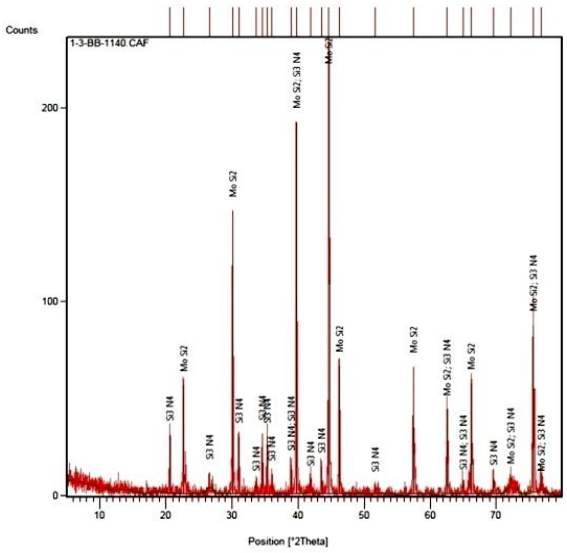

Figure 2. XRD patterns of composite (Si_3N_4-$MoSi_2$) sintered (sintering aid: 5wt% MgO, Press Pressure: 600 MPa, Max. Temperature: 1500ºC and 2h soaking time)

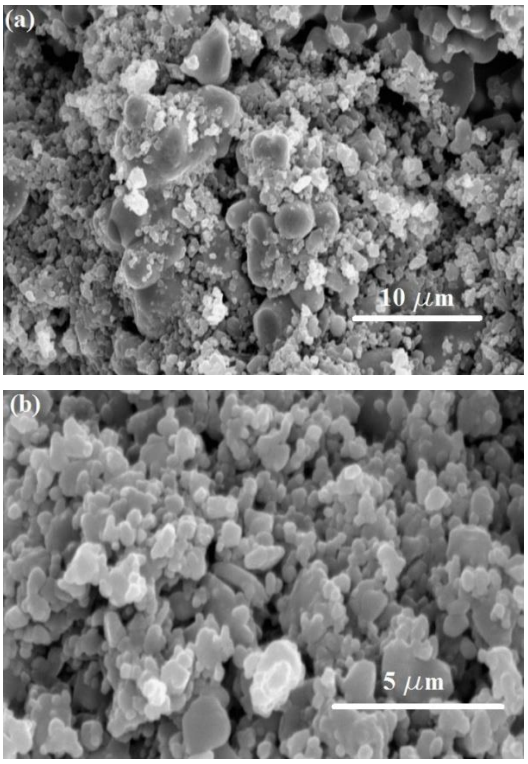

Figure 3.SEM micrographs of fracture surface of sample in secondary mode with two magnification: a- 3000 X and b- 8000 X (sintering aid: 5wt% MgO, Press Pressure: 600 MPa, Max. Temperature: 1500ºC and 2h soaking time)

3.2. MILLING

Part of the powders were milled using a Spex 8000 high energy mill before the pressing step. Table 2 shows

the effect of milling process on the densities of the green and final samples.

In addition, Figure 4 presents the green and sintered density diagrams of samples as a function of milled or unmilled raw materials.

It can be stated that the milling process of raw materials caused a significant increase in the final density of the samples, as seen in Table 2 and Figure 4.

The milling process also affects the microstructure of the samples. Figure 5 shows the SEM micrographs of Samples No. 3 and 7. According to this figure, sample No. 3 (un-milled) exhibits a coarser, more heterogeneous, and more porous than microstructure than sample No. 7 (milled).

In addition, Figure 6 shows the SEM micrographs of samples No. 6 and 8. In this figure (similar to Figure 5), sample No. 8 (milled) displays a finer and homogeneous microstructure than sample No. 6 (un-milled).

Milling, resulting from slipping together, not only reduces and refines the grain size of the raw materials but also increases the density (Figure 4) and microstructural homogeneity (Figure 5) of the samples. Moreover, the surface activity of the powder is increased by milling, which, in turn, enhances the final sample density (Singh et al., 2004).

TABLE 2. The effect of milling process on the green and final samples density and porosity

Sample No.	Milling Time (h)	RD green(%)	RD final(%)	Apprent Porosity(%)
3	0	65	77	22
7	1	75	78	21
6	0	73	65	33
8	1	77	85	14

3.3. SYNTERING AID

In this research, both values and types of sintering aids were studied.

3.3.1. SYNTERING AID VALUES

Samples No. 7 and 8 (containing MgO as the sintering aid) and No. 16 and 18 (containing Y_2O_3 as the sintering aid) were selected to investigate the effect of sintering aid on the density of the final sample.

Table 3 shows that the final density of the samples increased upon increasing the sinter aids value. Figure 7 demonstrates the SEM micrograph of samples No. 7, 8, and No. 16, 18. In this Figure, the microstructure of samples No. 8, 18 relatively more homogeneous with lower porosity, fewer detectable grain boundaries, fewer detectable individual grains, compared to sample No. 7, 16, respectively. These observations suggest that in these samples, the liquid phase was sufficiently produced and distributed within the sample microstructure during the sintering process due to the adequate sintering aid in these samples (German, 1996; German, 1985).

TABLE 3. The effect of the sintering aid value on the density and porosity of the final samples

Sample No.	Sintering Aid (type & percentage)	RD final (%)	Apprent Porosity(%)
7	5wt% MgO	78	21
8	10wt% MgO	85	14
16	5wt% Y_2O_3	76	23
18	10wt% Y_2O_3	81	18

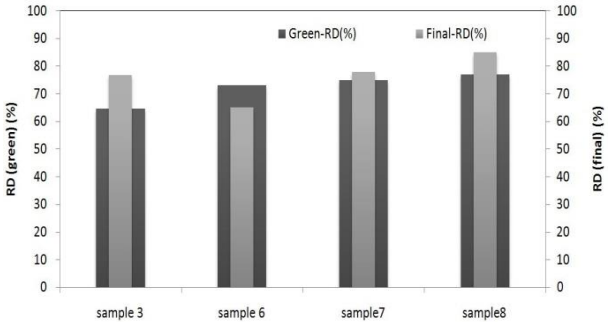

Figure 4. The effect of milling of raw materials on green and final samples density

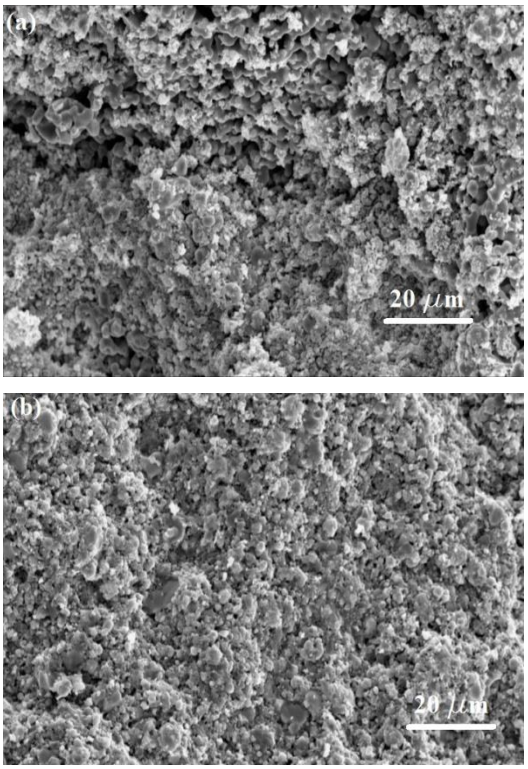

Figure 5. SEM micrographs of fracture surface of sample in secondary mode: a- No. 3 and b- no.7

3.3.2. SYNTERING AID TYPES

Liquid-phase properties such as viscosity, stability, and liquid-phase initiation temperature, among others, are related to the type of sintering aid used (Tayebifard, 2023; Heinrich et al., 2001). In this study, three types of synthesis aids were used in varying percentages (Table

4). Table 4 presents the final density and microhardness of the samples with similar preparation conditions but with different sintering aids used in their combinations. This table demonstrates that the sample containing milled raw materials and MgO as a sintering aid has a higher density than other samples. This is likely because MgO mixes well with other oxides (impurities) in these samples and is evenly distributed throughout the microstructure. Based on these assumptions, a homogeneous liquid phase is formed throughout the sample microstructure, resulting in higher or more controllable density in the samples (Figure 9). But why does this liquid phase form in samples doped with these additives? The sintering additive reacts with the oxygen-containing phases, such as SiO_2 or oxinitride, which are always present on the surface of commercially available Si_3N_4 powders, to form the liquid phase. Impurities in the starting powder are often also incorporated into this silicate melt as well (Ziegler et al., 1987).

As illustrated in Table 4, samples containing Y_2O_3, are characterized by less hardness than those with MgO and MgO-CeO_2. Accordingly, sample No. 8 demonstrates the best properties.

Non-homogeneous microstructure of these samples may account for their lower hardness (Figure 9). In Figure 8, the density and hardness of samples with various sintering aids are compared.

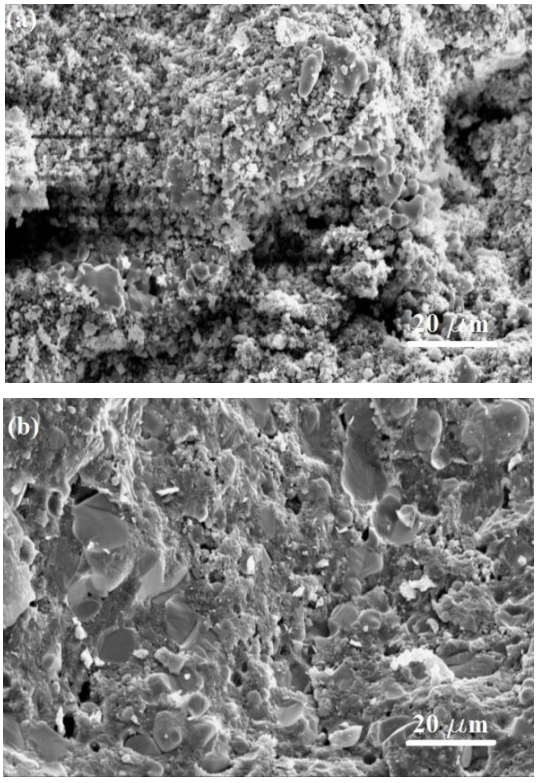

Figure 6. SEM micrographs of the fracture surface of samples in secondary mode: a- No. 6 and b- no.8

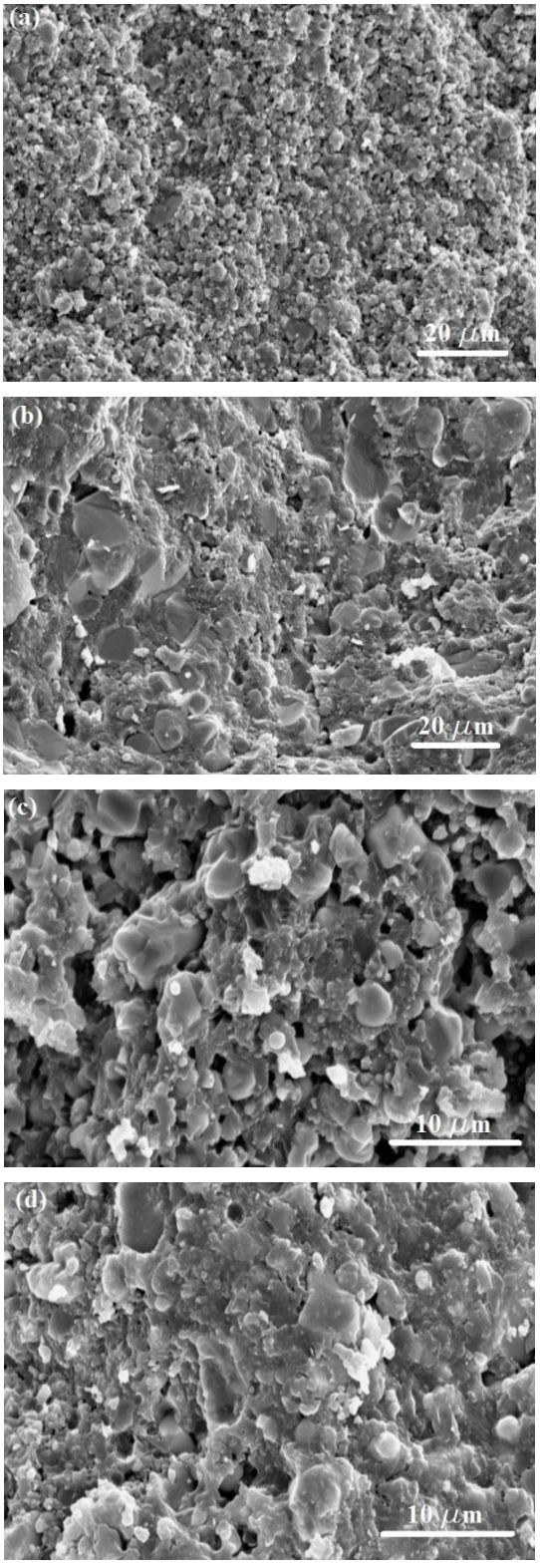

Figure 7. SEM micrographs of the fracture surface of samples in secondary mode: a- No. 7, b- No. 8, c- No. 16 and d- No. 18

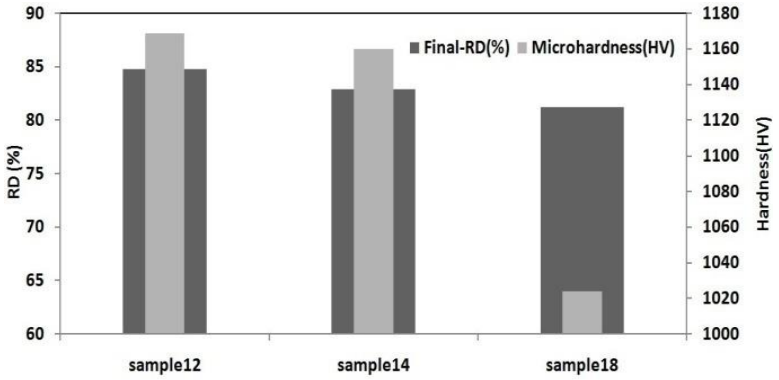

Figure 8. A comparison of the density and hardness of samples with various sintering aids

TABLE 4. The effect of the sintering aid type and soaking time on the densification and microharness of the final samples

Sample No.	Milling Time (h)	Sintering Aid (type & percentage)	Soaking Time (h)	RD final(%)	Apprent Porosity(%)	Microharness (HV)
7	1	5wt% MgO	2	78	21	-
8	1	10wt% MgO	2	85	14	1279
10	1	5wt% MgO	3	67	32	-
11	0	10wt% MgO	3	65	34	-
12	1	10wt% MgO	3	85	14	1169
13	0	5wt% MgO + 5wt% CeO_2	3	73	26	-
14	1	5wt% MgO + 5wt% CeO_2	3	83	15	1160
17	0	10wt% Y_2O_3	3	68	31	-
18	1	10wt% Y_2O_3	3	81	18	1024

Figure 9 shows the microstructure of the samples containing various sintering aids (as seen in Table 4). In this figure (9-a), the sample with MgO has a relatively homogeneous microstructure. As the sintering temperature rises, the spherical morphological phase becomes homogenously distributed. Figure 9b presents the microstructure of the sample containing MgO-CeO_2. In this sample microstructure, the matrix is homogeneous, and a small amount of visible porosity is present. Figure 9-c shows the microstructure of the sample containing Y_2O_3. This microstructure is not homogeneous, and the grains are not well-connected. It appears that the selected sintering temperature (1500°C) for this sample is insufficient to melt the glass phases containing Y_2O_3, leading to an incomplete and non-homogeneous final glass phase.

3.4. SOAKING TIME[1]

The density and microhardness of some samples sintered with different soaking times are compared in Table 4. These samples have similar composition and processing steps but vary in soaking times. Table 4 shows the final density of similar samples is not affected by soaking time; however, their hardness differ depending on the soaking time. For example, sample No. 12, with a soaking time of 3 hours, has lower hardness than sample No. 8, with a soaking time of 2 hours. The aspect ratio (l/d) is reduced with an increase in soaking time, where l is the length and d the diameter of the grain. Conversely, the mechanical properties of Si_3N_4, as a structural ceramic, improve with an increase in the percentage of β-phase, along with a higher aspect ratio. However, the increase in the soaking time leads to the growth of grain diameter, thus resulting in a reduction in the grain aspect ratio as well as the mechanical properties (Table 4) (German, 1996).

Figure 10 demonstrates the XRD patterns of samples No. 8 and 12. The analysis of these patterns confirms the presence of Si_3N_4 and $MoSi_2$ as the main phases in the desired composite. As evident in this figure, the presence of these phases is not affected at different soaking times.

Upon careful study of these patterns, several points can be understood. Table 5 shows the presence of α and β phases of samples No. 8 and 12. The table indicates that the α-Si_3N_4 score is higher than the β-Si_3N_4 score in both sample patterns. On the contrary, the β-phase score in sample No. 12 is higher relative that in sample No. 8. According to the reference, β-phase precipitates from the liquid phase (German, 1996). Therefore, increasing the soaking time can lead to an increase in the liquid phase during sintering and result in an increase of the β-phase score

[1]Time to keep the sample at maximum temperature

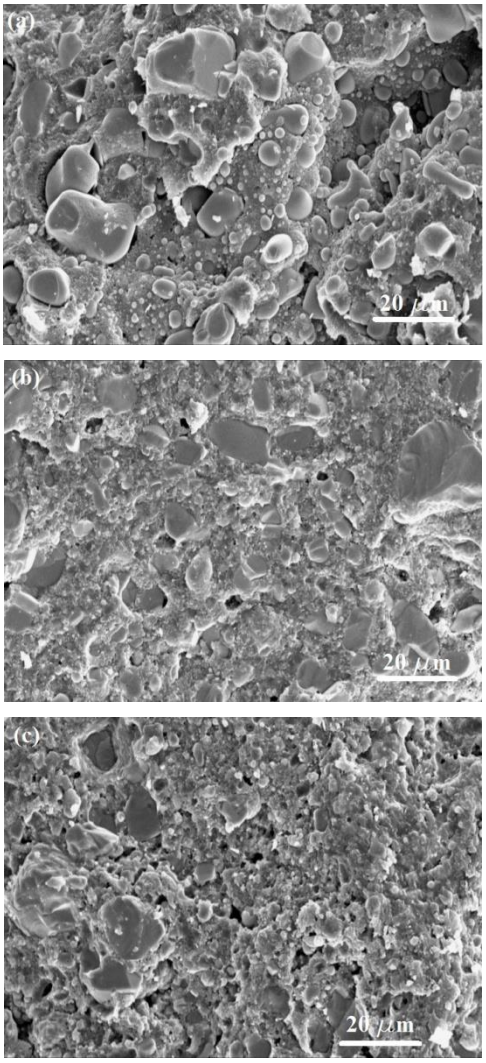

Figure 9. SEM micrographs of the fracture surface of samples in secondary mode: a- No. 12, b- No. 14, c- No. 18

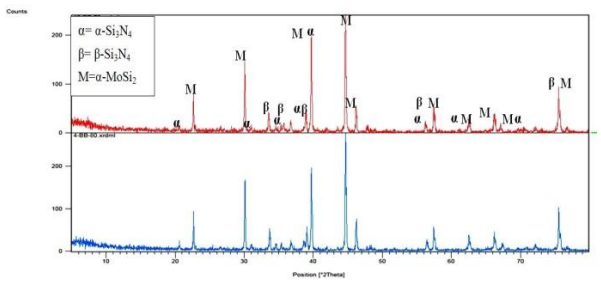

Figure 10. The XRD patterns of samples No. 8 and 12 (refer to Table 5)

TABLE 5. The effect of soaking time on score of types of the Si_3N_4 phases.

Sample No.	Soaking Time (h)	Score α-Si_3N_4	Score β-Si_3N_4	α/β (score)
8	2	12	2	6
12	3	15	8	1.88

Figure 11 presents the micrographs of samples No. 8 and 12. The significant difference between these two samples of microstructure is that in Figure 11-b, unlike Figure 11-a, some grains exhibit a spherical morphology. As mentioned earlier, the longer soaking time provides an opportunity for the grains to increase in diameter.

The reduction of the length-to-diameter ratio, which reflects the deformation of the pulled grains into a quasi-spherical shape, reduces the mechanical properties of the samples. For instance, this reduction is observed in the microhardness values shown in Table 4.

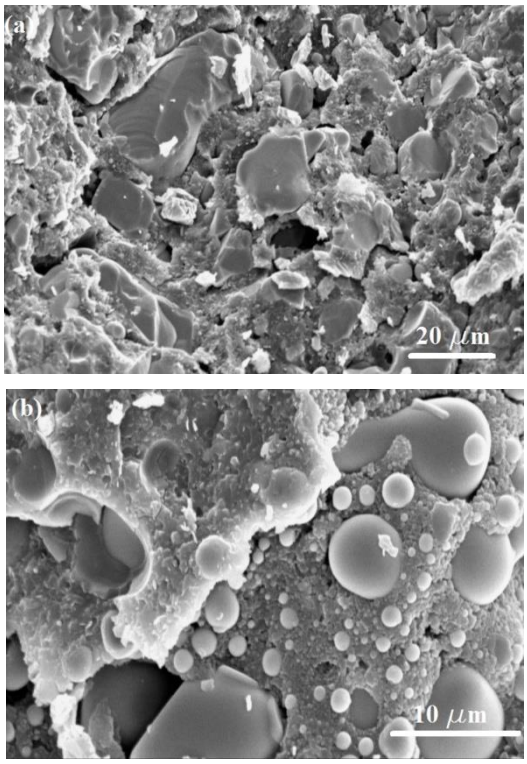

Figure 11. SEM micrographs of fracture surface of sample in secondary mode: a- No. 8, b- No. 12 (refer to table 5)

4. CONCLUSIONS

Increasing the compression pressure was an optimal approach to enhance the final density.

Milling of raw materials improved the final density as well as the homogeneity of the samples' microstructure.

The percentage and type of the sintering aid added to the raw material samples affected the densification and hardness of the final product. therefore, the sample No. 8 demonstrated the best properties.

An increase in the soaking time, although not affecting the sample density, resulted in an increase in the sample hardness due to higher aspect ratio and β-Si_3N_4 score.

Finally, these parameters were optimized in this research, resulting in the production of a composite with optimized porosity, homogeneity microstructure, favorable phase distribution, and optimum mechanical properties.

ACKNOWLEDGEMENTS

The author would like to acknowledge the financial support from Materials & Energy Research Center (MERC) of Iran for this research, based on grant number of 421392016.

REFERENCES

1. Angelo, P. C., & Subramanian, R. (2008). *Powder metallurgy: Science, technology and applications*. PHI Learning Pvt. Ltd. ISBN: 8120332814, 9788120332812. https://books.google.com/books/about/POWDER_METALLURGY.html?id=7cmb7BgZtvIC

2. Charfi, A., Ruttba, R., Kharrat, A. M., Wani, M. F., Dammak, M., & Sehgal, R. (2002). Friction and wear characterization of nanocomposites based on Si_3N_4 reinforced with SiC, Mo, and $MoSi_2$ nanoparticles. *Transactions of the Indian Institute of Metals*, *75*(3), 855–865. https://doi.org/10.1007/s12666-021-02494-1

3. Fasihi Dastjerdi, H., Tayebifard, S. A., Alizadeh, M., & Doroudian, M. (2012). Investigating the synthesis of $MoSi_2$ nanocrystal powder as a material capable of being used in industrial gas burners and jet turbine engines from commercial raw materials by self-propagating high-temperature synthesis (SHS). *Ith CNN, Shahrood*. https://civilica.com/doc/143255/

4. German, R. M. (1985). *Liquid phase sintering*. Springer Science & Business Media. ISBN: 978-1-4899-3601-1. https://link.springer.com/book/10.1007/978-1-4899-3599-1

5. German, R. M. (1996). *Sintering theory and practice*. John Wiley. ISBN: 978-0-471-05786-4. https://www.wiley.com/en-us/Sintering+Theory+and+Practice-p-9780471057864

6. German, R. M. (2005). *A-Z of powder metallurgy*. Elsevier. ISBN: 1856174298, 9781856174299. https://www.amazon.com/Powder-Metallurgy-Metal-Powders-Technology/dp/1856174298

7. Heinrich, J. G., & Aldinger, F. (2001). *Ceramic materials and components for engines*. John Wiley & Sons. Print ISBN: 9783527304165 | Online ISBN: 9783527612765 | https://doi.org/10.1002/9783527612765

8. Jankowiak, A., Valle, R., & Parlier, M. (2013). Potential of innovative ceramics for turbine applications. ODAS, Palaiseau, France. https://onera.hal.science/hal-01057786/document

9. Kota, N., Jana, P., & Roy, S. (2023). Elastic properties of porous silicon nitride fabricated via a low-temperature processing route. *Ceramics International*, *178*(49), 7066–7079. https://doi.org/10.1016/j.ceramint.2022.10.046

10. Lai, J., Kadin, Y., & Vieillard, C. (2018). Characterization and modelling of the degradation of silicon nitride balls with surface missing-material defects under lubricated rolling contact conditions. *Wear*, *398–399*, 48–54. https://doi.org/10.1016/j.wear.2017.12.007

11. Liu, Y., Xin, R., He, F., Qiu, & You, Zh. (2022). Novel approach to prepare Fe-TiN cermets from ilmenite concentrate using clean NH_3 gas. *International Journal of Refractory Metals and Hard Materials*, *108*, 105943. https://doi.org/10.1016/j.ijrmhm.2022.105943

12. Lizuka, T., Murao, T., Yamamoto, H., & Kita, H. (2002). Microstructures and properties of Mo_5Si_3-particle-reinforced Si_3N_4-matrix composites. *Journal of the American Ceramic Society*, *85*(4), 954–960. https://doi.org/10.1111/j.1151-2916.2002.tb00198.x

13. Ramachandra Rao, R. (2023). Dielectric constant and flexural strength of micro-porous slip-cast partially sintered silicon nitride. *Ceramics International*, *48*(23, Part B), 35927–35936. https://doi.org/10.1016/j.ceramint.2022.10.002.

14. Sciti, D., Guicciardi, S., & Bellosi, A. (2002). Microstructure and properties of Si_3N_4–$MoSi_2$ composites. *Journal of Ceramic Processing Research*, *3*(3), 87–95. http://www.jcpr.or.kr/journal/archive/view/90

15. Shahbazi, M., Tayebifard, S. A., & Razavi, M. (2016). Effect of Ni content on the reaction behaviour and microstructure of TiB_2–TiC/Ni cermets synthesized by MASHS. *ACERP*, *2*(2), 22–26. https://doi.org/10.30501/ACP.2016.70020

16. Singh, S., Godkhindi, M. M., Krishna Rao, R. V., & Murty, B. S. (2004). Effect of mechanical activation on synthesis of ultrafine Si_3N_4–$MoSi_2$ in situ composites. *Materials Science and Engineering A*, *382*, 321–327. http://dx.doi.org/10.1016/j.msea.2004.05.015

17. Tapia-López, J., & Pech-Canul, M. I. (2023). Processing, microstructure, properties, and applications of $MoSi_2$-containing composites: A review. *Frontiers in Materials*, *10*, 1165245. https://doi.org/10.3389/fmats.2023.1165245.

18. Tayebifard, S. A. (2023). *Non-oxide engineering ceramics*. Coarse Note, Materials and Energy Research Center. http://faculty.merc.ac.ir/tayebifard/

19. Yang, J. F., Zhang, G. J., & Ohji, T. (2001). Fabrication of low-shrinkage, porous silicon nitride ceramics by addition of a small amount of carbon. *Journal of the American Ceramic Society*, *84*, 1639–1641. https://doi.org/10.1111/j.1151-2916.2001.tb00890.x

20. Ziegler, G., Heinrich, J., & Wotting, G. (1987). Review relationships between processing, microstructure, and properties of dense and reaction-bonding silicon nitride. *Journal of Materials Science*, *22*, 3041–3086. https://doi.org/10.1007/BF01161167